

Exploring the Connection between UV/Optical Variations and Radio Emission in Radio-Quiet Quasars: Clues on Radio Emission Origin

Mai Liao,^{1,2★} Junwan Wang,^{1,2†} Wenyong Kang^{1,2} Minhua Zhou³

¹CAS Key Laboratory for Research in Galaxies and Cosmology, Department of Astronomy, University of Science and Technology of China, Hefei, Anhui 230026, China

²School of Astronomy and Space Science, University of Science and Technology of China, Hefei 230026, China

³School of Physics and Electronic Information, Shangrao Normal University, 401 Zhimin Road, Shangrao 334001, China

Accepted 2022 January 26; Received 2021 December 30; in original form 2021 October 15

ABSTRACT

The radio emission in radio-quiet quasars (RQQs) has been a long mystery and its physical origin remains unclear. In a previous work we find UV/optical more variable quasars have stronger X-ray emission, indicating a link between disc turbulence and X-ray corona heating. In this work, for the first time, we investigate the relation between UV/optical variability and the radio emission in RQQs selected from SDSS stripe 82 and FIRST radio survey. We median stack the FIRST images and detect clear signals from RQQs in the co-added images of individually radio non-detected sources. Controlling the effects of other parameters, including redshift, black hole mass, bolometric luminosity and Eddington ratio, we find more variable RQQs, which are known to be X-ray relatively brighter, show tentatively weaker radio emission, contrary to the linear X-ray/radio correlation if the radio emission is from or driven by the corona. The discovery also suggests that if the radio emission in RQQs is driven by AGN activity (such as weak jet), the underlying driving process is independent to the disc turbulence which drives UV/optical variability and probably also corona heating. Alternatively, the radio emission could be due to star formation in the host galaxies.

Key words: accretion, accretion discs — galaxies: active — quasars: general — X-ray: galaxies — radio continuum: galaxies.

1 INTRODUCTION

Quasars, powered by the central accreting supermassive black holes, emit light throughout the entire electromagnetic spectrum from radio to X-rays and γ -rays. Traditionally, based on the radio emission loudness which is defined as the ratio between radio and optical flux (e.g., $R = f_{5\text{GHz}}/f_{4400}$, Kellermann et al. 1989), quasars could be divided into the two populations of radio-loud (RL) and radio-quiet (RQ) (e.g., Padovani et al. 2017; Panessa et al. 2019). But see Padovani (2017) for an alternative naming of RL/RQ as ‘jetted’ and ‘non-jetted’. Powerful relativistic and well collimated jets (e.g., Blandford et al. 2019; Hardcastle & Croston 2020) are commonly presented in radio-loud quasars (RLQs), which account only approximately 10–20% (e.g., Kellermann et al. 1989; Ivezić et al. 2002) of the whole population. The radio emission of the rest majority (i.e., radio-quiet quasars, RQQs) is typically 1000 times fainter (e.g., Miller et al. 1993; Panessa et al. 2019), the origin of which is still under debate. Possible physical origins of the radio emission in RQQs include low-power compact jets, accretion-disc corona, outflows, and star formation in the host galaxies (e.g., Padovani 2016; Panessa et al. 2019).

Resolving the expected extended, diffuse radio emission associated with star formation in the host galaxies of distant RQQs is much more challenging than that in nearby lower luminosity radio-quiet AGN (e.g., VLA and eMERLIN observations of NGC 1614, Olsson

et al. 2010). The commonly detected compact radio structures on arc-second scales in RQQs (e.g., Ulvestad et al. 2005; Leipski et al. 2006; Smith et al. 2020) are often insufficient to separate radio emission originating from star-formation and AGN-related activity. Comparing the radio power in RQQs with the star formation activities in their host galaxies also yielded mixed results, with some favoring the star formation origin (e.g. Bonzini et al. 2015; Kellermann et al. 2016; Gürkan et al. 2019) and others favoring black hole activity (e.g. Zakamska et al. 2016; White et al. 2017).

AGN driven radio emission in RQQs could be immediately confirmed if the linear jet-like structures, which may be a scaled-down version of the more powerful ones in RLQs (e.g., Falcke & Biermann 1995; Panessa et al. 2019; Macfarlane et al. 2021), could be directly resolved (e.g., Kellermann et al. 1994; Kukula et al. 1998; Blundell & Rawlings 2001; Blundell et al. 2003; Ulvestad et al. 2005; Leipski et al. 2006; Wang et al. 2021). The observed flat radio spectra and the high-brightness temperature ($> 10^7$ K) of the compact radio cores also favor the non-thermal processes from relativistic electrons usually related with jets (e.g., Blandford & Königl 1979; Blundell & Beasley 1998; Ulvestad et al. 2005; Panessa & Giroletti 2013). However, although lower power jets have been detected in a handful of RQQs, most RQQs studies with high-resolution radio observations show unresolved radio structures, even at milli-arcsecond scales by VLBI imaging (e.g., Ulvestad et al. 2005). The uncollimated jets, i.e., outflows, might also contribute to the radio emission in RQQs. They may produce radio emission with non-isotropic, conical and spatially extended structures (Panessa et al. 2019), and has been proposed to explain the observed correlation between the velocity width of [O III]

★ E-mail: liaomai@ustc.edu.cn

† E-mail: jxw@ustc.edu.cn

and the radio emission in RQQs (Mullaney et al. 2013; Zakamska & Greene 2014; Hwang et al. 2018).

Accretion-disk corona is also an option for radio emission origin of RQQs (Laor & Behar 2008; Raginski & Laor 2016), as the evidence showed in Laor & Behar (2008) that 71 radio-quiet PG quasars follow the well-established relation of $L_{\text{R5GHz}}/L_X \sim 10^{-5}$ in coronally active cool stars (Guedel & Benz 1993). Meanwhile, the detections of millimeter excess emission (100-300 GHz) in a few local Seyfert galaxies suggest the existence of a compact, optically thick core, which could be associated with the corona (Behar et al. 2018; Inoue & Doi 2018). Recently it was found X-ray luminosity of radio-quiet PG quasars correlate more tightly with the 45-GHz luminosity than the 5-GHz (Baldi et al. 2021), suggesting the 45-GHz emission originates probably from the accretion disc corona. High-frequency observations for more RQQs however are challenging due to the weakness of the signal. Furthermore, studies on the correlation between X-ray and radio emission (at any frequency) in larger samples of RQQs are scarce.

In this work we explore the physical origin of radio emission in RQQs from a new perspective, i.e., to study the relation between radio emission and UV/optical variability in a large sample of RQQs. Aperiodic variability from radio to γ -ray, over a wide range of timescales from minutes to years, is one of the prominent characteristics of quasars (Padovani et al. 2017). In UV/optical, the variability is generally attributed to random fluctuations in the accretion disc, probably driven by magnetic turbulence (e.g. Kelly et al. 2009; Cai et al. 2016, 2018; Kang et al. 2018). Remarkably, Kang et al. (2018) found a intrinsic link between X-ray loudness (defined as L_X/L_{bol}) and UV/optical variability amplitude in normal quasars, i.e., more variable quasars have stronger X-ray emission, suggesting a physical link between disk turbulence and corona heating. Thus exploring the connection between UV/optical variability and radio emission enables us to at the same time study the connection of X-ray and radio emission in a large sample of RQQs. If radio emission in RQQs is dominated by the corona activity, we thus expect more variable quasars should also have stronger radio emission. Furthermore, the UV/optical variability is a feature intrinsic to the accretion process. Examining the correlation between radio emission and UV/optical variability is useful to determine whether the radio emission is associated with such nuclear activities. Such correlation, if exists, could yield new clues to the understanding of radio emission origin.

In this paper, we explore such connection using SDSS stripe 82 quasars within FIRST survey footprint. We stack FIRST images of quasars to measure the average radio emission. The outline of our work is as follows: §2 presents the sample and the stacking analyses of radio images; §3 presents our results; §4 provides a discussion. Throughout the paper, the cosmological parameters $H_0 = 70 \text{ km s}^{-1} \text{ Mpc}^{-1}$, $\Omega_m = 0.3$, and $\Omega_\lambda = 0.7$ are adopted.

2 SAMPLE AND STACKING ANALYSIS

2.1 The quasar sample

In order to build quasar sample with UV/optical variability measurements, we start from the SDSS Stripe 82 survey which covers about 290 deg^2 equatorial field of the sky and has been scanned over 60 times in the *ugriz* bands by Sloan Digital Sky Survey (Sesar et al. 2007). MacLeod et al. (2012) provided the re-calibrated ~ 10 years long light curves in *ugriz* for 9258 spectroscopically confirmed

quasars in SDSS Data Release 7 (SDSS DR7)¹. 9120 out of them are located within the footprint of the Faint Images of the Radio Sky at Twenty-Centimeters (FIRST) survey, which is conducted with NRAO Very Large Array (VLA) in its B-configuration centered at 1.4 GHz and covers about 10,575 square degrees² (Becker et al. 1995; Helfand et al. 2015). The FIRST images have a resolution of $\sim 5''$, and a typical rms sensitivity of 0.15 mJy. We cross-match with the FIRST catalog (Helfand et al. 2015) with a matching radius of $5''$, and find 517 (5.7%) sources with FIRST counterparts. Among the FIRST detected sources, $\sim 80\%$ could be classified as radio-loud based on their radio-loudnesses. This indicates while the dominant population of the sample is radio-quiet, some ($\sim 6\%$, assuming $\sim 10\%$ of the 9120 quasars are radio-loud) radio non-detected sources could still be radio-loud.

We further match the quasars with Shen et al. (2011) to obtain their z , M_{BH} , L_{bol} and R_{edd} , where we adopt the fiducial virial M_{BH} from their catalog. 108 objects are further rejected due to the lack of M_{BH} .

We adopt the same method as in Kang et al. (2018) to measure the intrinsic variability amplitude in each photometric band for each quasar. The variation amplitude is defined as excess variance σ_{rms} (e.g., Sesar et al. 2007; Zuo et al. 2012) as follows:

$$\sigma_{\text{rms}}^2 = \frac{1}{N-1} \sum (X_i - \bar{X})^2 - \frac{1}{N} \sum \sigma_i^2 \quad (1)$$

where N is the number of photometric measurements for a single light curve, X_i the magnitude for i_{th} observation, \bar{X} the average magnitude, and σ_i the i_{th} photometric uncertainty of each observation. We exclude *u* and *z* band data due to their significantly larger photometric uncertainties when compared with other three bands of *gri*. With only keeping the ones which have at least 20 epochs in each of the light curve to ensure accurate measurement of σ_{rms} , our final sample consists of 8819, 8829, 8826 RQQs with UV/optical variability amplitude in *g*, *r*, *i* band, respectively. Below we focus on *g* band data as quasars are generally more variable in *g* band than in *r* or *i* band. Unless otherwise stated, we present below the results using *g* band σ_{rms} , which are further verified by the well consistent results obtained using *r* or *i* band data.

2.2 High-/low-variability subsamples

In order to study the relation between radio emission and UV/optical variations in RQQs, we firstly divide our quasars equally into two subsamples according to σ_{rms} , that is, a high-variability and low-variability subsample (hereafter HVQ0 and LVQ0 respectively).

However it is known that the UV/optical variability amplitude of quasars depends on physical parameters including luminosity, SMBH mass, Eddington ratio, and redshift (e.g. see Kang et al. 2018, 2021, and references therein). Indeed, according to Kolmogorov-Smirnov (K-S) test, the HVQ0 and LVQ0 subsamples we obtained above do have significantly different distributions in redshift, bolometric luminosity, SMBH mass and Eddington ratio, and LVQ0s have on average higher redshift, luminosity, SMBH mass and Eddington ratio (see Fig. 1). The radio flux in RQQs could also be sensitive to these parameters. A fair comparison to reveal the intrinsic connection between UV/optical variability and radio emission in RQQs should be made with these parameters matched.

As the stacked signals would be too weak if we split the samples

¹ http://faculty.washington.edu/ivezic/cmacleod/qso_dr7/Southern.html

² <http://sundog.stsci.edu>

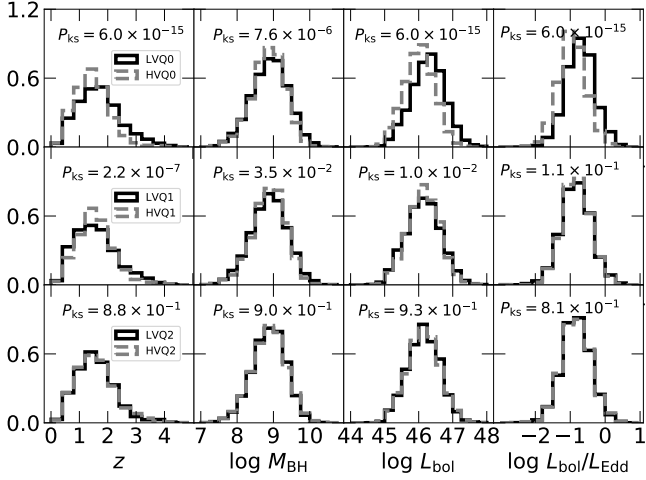


Figure 1. The distributions of z , M_{BH} , L_{bol} and R_{edd} for HVQ0/LVQ0, HVQ1/LVQ1, HVQ2/HVQ2 from upper to lower panels, respectively. The K-S test results between the distributions are given in the plot.

into too many small bins in the multidimensional space of these parameters, we adopt two different approaches to divide the parent sample again into just two subsamples but with the parameters aforementioned matched between them. We first follow [Kang et al. \(2018\)](#) to perform multiple linear regression as follows:

$$\sigma_{\text{rms}} \sim M_{\text{BH}}^a R_{\text{edd}}^b (1+z)^c \quad (2)$$

We derive the residual σ_{rms} for each source from above equation, i.e., the difference between the observed σ_{rms} and the expected one based on the best-fit regression (see Fig. 2). And we divide the parent sample again into low-variability quasars (hereafter LVQ1) and high-variability quasars (HVQ1) based on the residual σ_{rms} . The HVQ1 and LVQ1 subsamples do show consistent distributions of bolometric luminosity, SMBH mass and Eddington ratio (see Fig. 1), however the match in their redshift distributions is poor, likely because the dependence of σ_{rms} on redshift is more intricate than Equation 2 could describe³.

We then adopt a different approach to build HVQ and LVQ samples with better matched parameters. We randomly choose as many as possible and equal number of HVQ1s and LVQ1s (defined according to residual σ_{rms} in Fig. 2) in each three-dimensional bin of z , M_{BH} , and L_{bol} ⁴ which contain both HVQ1s and LVQ1s. We endeavor to adjust the bins sizes of z , M_{BH} , and L_{bol} to maximize the number of sources selected. Finally, we could select $\sim 88\%$ sources out of the parent sample into HVQ2 and LVQ2 subsamples. This is because with the grid selection approach when unequal numbers of LVQ1s and HVQ1s fall in a grid, we have to drop sources to select equal number of LVQ1s and HVQ1s (e.g. see [Zhou & Gu 2021](#)). As expected, the HVQ2 and LVQ2 subsamples derived with this approach show statistically consistent distributions in z , M_{BH} , and L_{bol} and R_{edd} (see Fig. 1).

³ Various lines which would shift into or out of SDSS g band at certain redshifts could alter the values of σ_{rms} as the lines are less variable than the underlying continuum emission, leading to sharp dependence of σ_{rms} on redshift.

⁴ Here, using R_{edd} to replace L_{bol} would obtain same results.

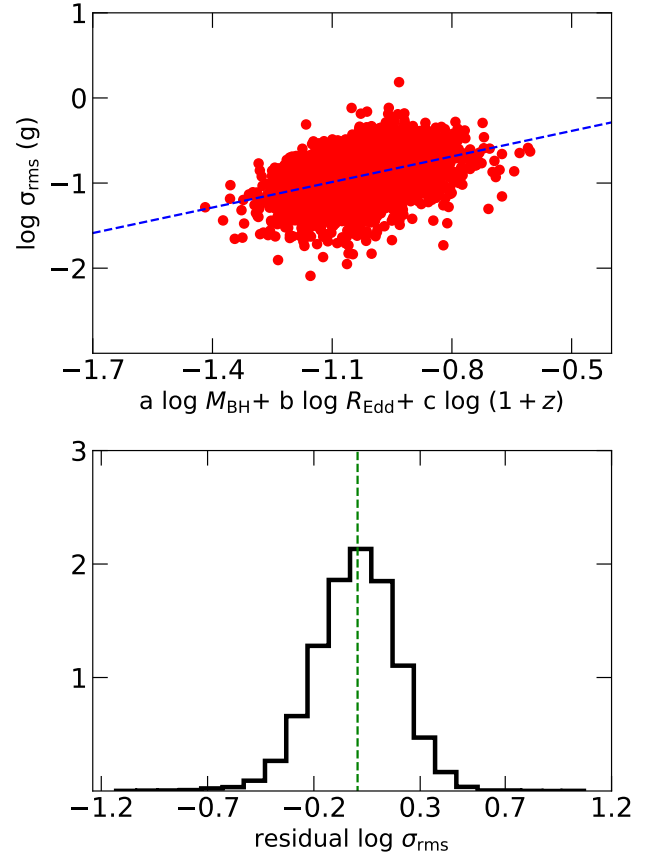


Figure 2. Upper: the observed SDSS g band σ_{rms} versus the expected value based on the best-fit correlation (blue dashed line) in equation 2. Lower: the distribution of the residual σ_{rms} (observed minus expected). The vertical green dashed line marks the segmentation between HVQ1 and LVQ1.

2.3 FIRST image stacking

Below we describe the procedures we adopted to derive the stacked FIRST image of a sample of quasars. We extract from FIRST survey the radio cutout image for each quasar centred on the SDSS quasar position (with size of $30'' \times 30''$, pixel size $1.8''$). As most of our quasars are individually non-detected by FIRST, we employ the method of image stacking, a technique for combining data from many individual sources in order to study their statistical properties which are below the detection limit for a particular survey (e.g., [White et al. 2007](#); [Garn & Alexander 2009](#)), to obtain the average radio emission. In this work, we adopt the median stacking approach, which is insensitive to outliers (i.e., the tails of the underlying flux distribution) and more robust for non-Gaussian distributions when compared with mean stacking ([White et al. 2007](#)). We align and median stack the individual FIRST images on a pixel-by-pixel basis ([Radcliffe et al. 2021](#)), using the python code of `numpy.ma.median` ([van der Walt et al. 2011](#)). The average radio flux density of a sample could then be derived from the stacked image. As a point-like source is centered at the nominal quasar(s') position in each co-added image (see §3) and the changing PSFs from various individual FIRST images in the

stacking are not CLEANed⁵, following White et al. (2007), we use peak flux density only from the central pixel in each co-added image.

Another advantage of median stacking, when compared with mean stacking, is that the average radio flux derived from median stacking is less sensitive to the small population of radio-loud sources, and could better represent the dominant radio-quiet population. Note the FIRST images are not sufficiently deep to detect/exclude all radio-loud quasars from our sample. To further minimize the effect of the small population of FIRST non-detected but radio-loud sources, we derive the 45th percentile⁶ instead of the simple median (50th percentile) while stacking FIRST images, to reduce the effect of the $\sim 10\%$ radio-loud population. This is practically valid because some radio-loud sources, though non-detected, may have marginal/tentative signals in FIRST images, and thus the radio-loud fraction is expected to be even lower (or negligible) in sources with apparent FIRST pixel values in the bottom 45%. Note this approach (45th percentile) could only yield perfect measurement of average radio flux for RQs (free from contamination by radio-loud ones) if the radio-loud fraction is 10% in the whole sample, and none of the sources with FIRST pixel values in the bottom 45% is radio-loud. Hereafter we refer the 45th percentile of the whole sample (including those FIRST detected) as the median of RQs, if not otherwise specified.

We finally stress that directly adopting the median of the whole sample (instead of 45th percentile) would yield slightly higher average radio flux densities, however, it won't alter the main results of this work. Using mean stacking would not change the key results presented in this paper either.

3 RESULTS

Fig 3 shows the co-added FIRST images for H/LVQ (0/1/2). Clear compact radio signals are visible in the co-added images, showing the stacking approach is able to detect the average radio emission from our large sample of RQs. The asymmetric error bars for each peak flux density were derived using the bootstrapping technique described in Karim et al. (2011). It should be noted that our measurements of flux density values were not corrected for FIRST snapshot bias which exists for FIRST faint sources and our values above should be corrected by a multiplier of 1.4 (see details in White et al. 2007). As we aim to study the difference between subsamples, the snapshot bias would not affect our results.

The median-stacked flux densities of H/LVQ (0/1/2) are plotted in Fig. 4. The radio emission of the HVQ0 subsample is tentatively weaker (with a S/N of 1.7) compared with LVQ0 ($28.3^{+3.2}_{-3.6} \mu\text{Jy}$ vs $36.5^{+2.5}_{-3.4} \mu\text{Jy}$). Similar trends are seen in the comparisons between

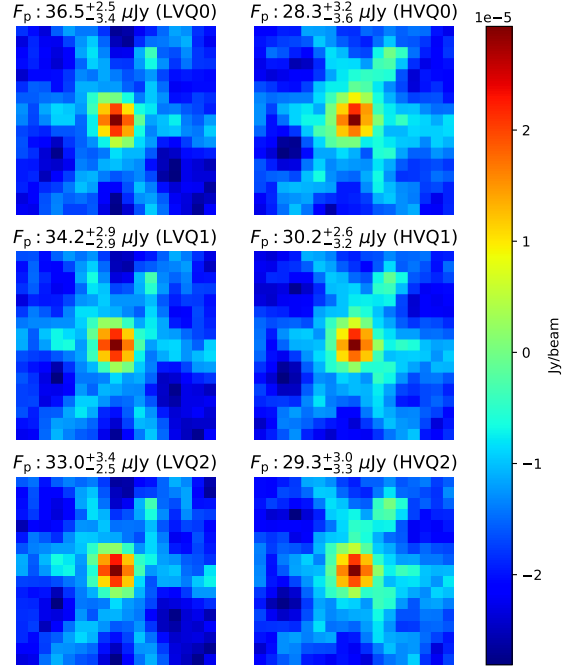


Figure 3. The co-added 1.4 GHz FIRST images of low-variability and high-variability RQs (from upper to lower panels, respectively, for LVQ0s and HVQ0s, LVQ1 and HVQ1, and LVQ2 and HVQ2). The peak flux densities indicated by the central pixel in each stacked image are shown at the top of each image. All the co-added images have a scale of $30'' \times 30''$ with pixel size $1.8''$. The sidelobe effects are apparent due to the uncleaned PSFs.

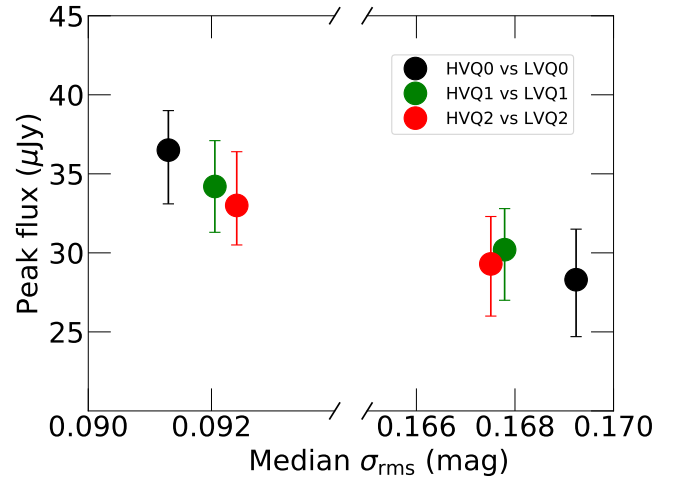


Figure 4. The median radio flux densities for HVQ0 and LVQ0 (black dots), HVQ1 and LVQ1 (green dots), and HVQ2 and LVQ2 (red dots).

⁵ Although the most commonly used method to restore the flux density of a radio source from dirty image is CLEAN, maximum entropy and compressed sensing (Thompson et al. 2017), the flux density of a radio source can also be derived from the peak flux density in dirty beam when the source is very compact (i.e. point source). Since our RQs are individually non-detected, their CLEANed images are not available. To avoid the problems caused by the fact that the PSF in the median stacked image is some kind of combination of various individual PSFs and it is not a CLEAN Gaussian, it is simpler to just use the value of central pixel as the peak flux density (Richard L. White, private communication).

⁶ For each pixel in FIRST images to be stacked, we rank the flux densities in the pixel from all quasars in a sample, drop the 10% with largest flux densities, and derive the median for the rest 90%.

HVQ1 and LVQ1 ($30.2^{+2.6}_{-3.2} \mu\text{Jy}$ vs $34.2^{+2.9}_{-2.9} \mu\text{Jy}$), and between HVQ2 and LVQ2 ($29.3^{+3.0}_{-3.3} \mu\text{Jy}$ vs $33.0^{+3.4}_{-2.5} \mu\text{Jy}$).

SDSS Stripe 82 is also covered by the 1.4 GHz VLA survey of the SDSS Southern Equatorial Stripe (VLA-Stripe 82, [Hodge et al. 2011](#)), with an angular resolution of $1.8''$ and a rms sensitivity of $\sim 50 \mu\text{Jy}$ over 92 deg^2 . The VLA-Stripe 82 provides us considerably deeper radio images with better resolution, but for a smaller sample of quasars. Among the 3799 quasars within the footprint of VLA-Stripe 82, 280 ($\sim 7.4\%$) have radio detections. Cross-matching the 3799 quasars with [Shen et al. \(2011\)](#) to obtain M_{BH} , L_{bol} , R_{edd} and excluding sources with < 20 epochs in SDSS g band light curves, we obtain a sample of 3669 quasars. We repeat our sample splitting, and radio imaging stacking analyses using radio images from VLA-Stripe 82 for this sample. The results are presented in Fig. 5, with the derived median radio flux densities well consistent (within statistical errors) with those obtained using FIRST images (Fig. 3 and 4).

In above analyses we have adopted the 45th percentile while stacking radio images to minimize the contamination by the $\sim 10\%$ radio-loud sources in the quasar sample. Alternatively and more conservatively, we could use only quasars which can be safely classified as radio-quiet based on available radio fluxes or upper limits, and use such sample for analyses. We adopt an upper limit of 1 mJy at 1.4 GHz for FIRST non-detections, and 0.3 mJy for VLA-Stripe 82 non-detections. We utilize the rest-frame 2500 Å flux from [Shen et al. \(2011\)](#), and assume a radio spectra index of $\alpha = 0.5$ to estimate the radio-loudness $f_{5\text{GHz}}/f_{2500\text{\AA}}$ (with a threshold of < 10 for radio-quiet sources). We find 5476 out of 8819 quasars with FIRST coverage could be safely classified as radio-quiet, including 106 with FIRST detections. With deeper VLA-Stripe82 images, 3410 out 3669 quasars remain, including 71 radio detections. Repeating our analyses (sample splitting and radio image stacking) using these samples, we present the simple median flux densities for low- and high-variability subsamples in Fig. 6. Clearly, we see similar trends that HVQs have tentatively weaker radio emission compared with LVQs. Not the absolute flux densities in Fig. 6 from the FIRST sample are considerably higher than those plotted in Fig. 4 and 5. This is mainly because to ensure the radio quietness based on radio flux upper limit, the quasars we kept need to have higher luminosity and/or lower redshifts, thus higher average radio fluxes. For the VLA-Stripe82 sample, 93% sources are kept as radio-quiet as VLA-Stripe82 images are sufficiently, thus the median fluxes plotted in Fig. 6 are somehow effectively 46.5th percentile, thus only slightly higher than 45th percentile.

In summary, we find high-variability RQQs (with matched redshift, bolometric luminosity and SMBH mass) have tentatively weaker radio emission compared with low-variability ones.

4 DISCUSSION

4.1 The origin of radio emission in RQQs

[Kang et al. \(2018\)](#) investigated the relation between UV/optical variation amplitude (σ_{rms}) and X-ray loudness (L_X/L_{bol}) using a sample of X-ray detected quasars in Stripe 82X ([Ananna et al. 2017](#)). They found that quasars with more intense X-ray radiation (controlling the effects of other physical parameters, i.e., z , M_{BH} , L_{bol} and R_{edd}) are more variable in the UV/optical. It can be interpreted that the UV/optical variations and X-ray emission are both associated with magnetic turbulence, i.e., the stronger disk turbulence, the more energy can be dissipated into the corona which could be heated through magnetic reconnection. We divide the sample of [Kang et al. \(2018\)](#)

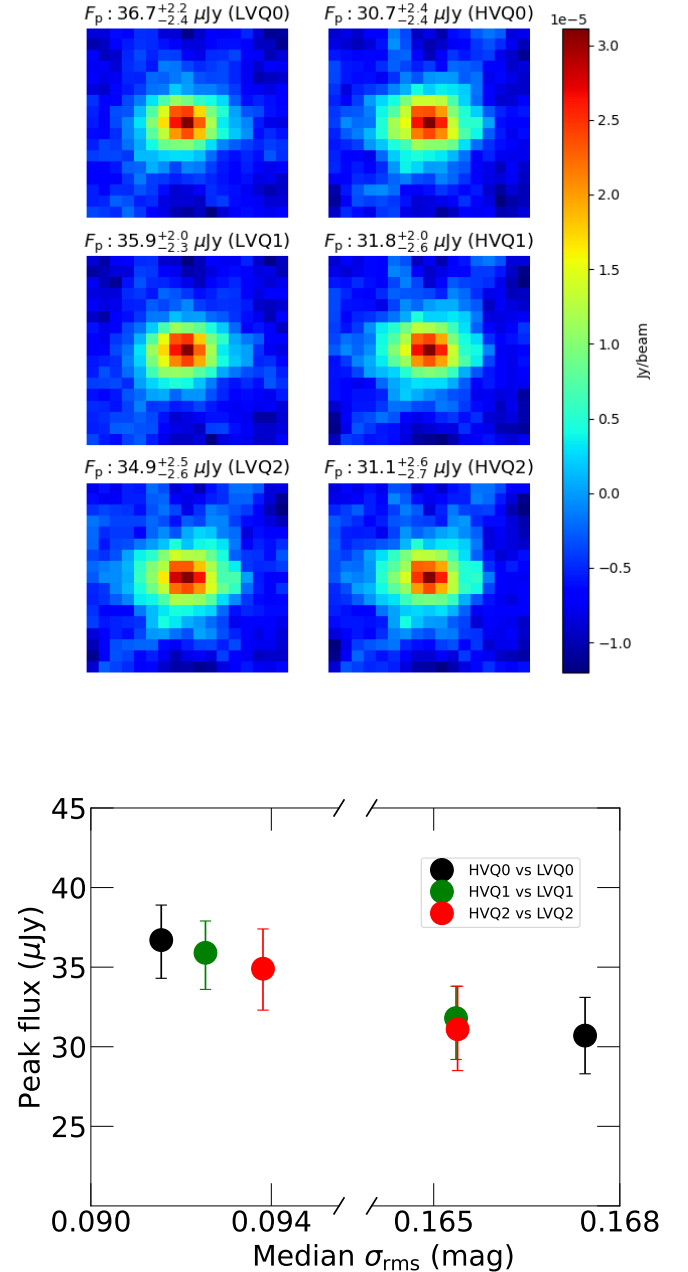


Figure 5. The stacked 1.4 GHz VLA images (upper, with a scale of $10'' \times 10''$ and pixel size of $0.6''$) of low- and high-variability quasars and derived median radio flux densities (lower), for quasars within the footprint of VLA-Stripe 82 which is considerably deeper than FIRST, but covering a smaller sky area.

into high- and low-variability quasars as we built HVQ1 and LVQ1 in this work. We find that while the HVQ1 sample of [Kang et al. \(2018\)](#) is more variable than LVQ1 by a factor of 1.80 (which is similar to the difference between our LVQ1/HVQ1 and LVQ2/HVQ2), their HVQ1 are X-ray brighter on average by a factor of 1.5 than LVQ1.

The radio emission is expected to linearly correlate with X-ray according to the relation between X-ray and radio emission with $L_R = 10^{-5} L_X$ in RQQs reported in [Laor & Behar \(2008\)](#), probably driven by the Neupert effect (where $L_R = dL_X/dt$ as detected in

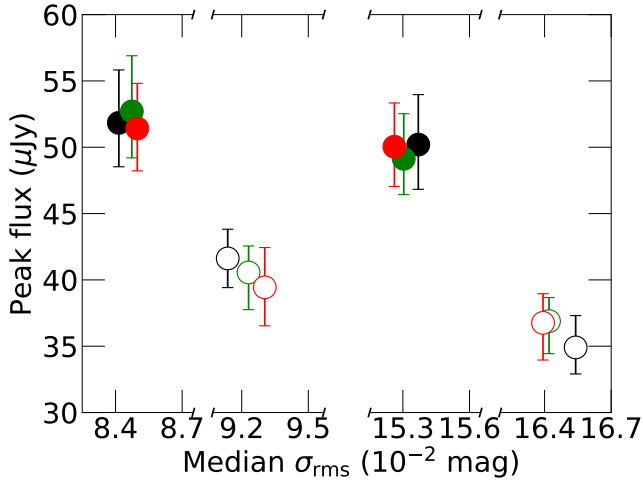


Figure 6. Similar to Fig. 4 and 5, but for quasars which can be safely classified as radio-quiet based on radio fluxes or upper limits. Solid and open symbols (with colors same to Fig. 4) are derived using FIRST and VLA-Stripe82 images, respectively.

stellar coronae, Neupert 1968; Guedel & Benz 1993). If so, we would expect our HVQ2 have radio emission ~ 1.5 times stronger than LVQ2. However, our results show that the radio emission of HVQs are consistent with that of LVQs, contrary to the prediction (see the left panel in Fig. 7).

Our discovery thus indicates the 1.4 GHz FIRST radio emission of RQs is unlikely driven by the central corona, or an extended region powered by the central corona. It would be intriguing to explore in the future the connection between UV/optical variability (thus X-ray loudness) and radio emission at higher frequencies, where the contribution of the corona to radio emission could be more significant.

On the other hand, if the radio emission in RQs is dominated by weak jet, our discovery suggests that such jet should be driven by processes other than those which drive the UV/optical variability and corona heating. Note Cai et al. (2019) suggested that the inner accretion disk of RLQs fluctuates less compared with RQ ones, likely because the stronger magnetic field in RLQs could stabilize the inner disc, i.e., implying a negative link between jet power and UV/optical variability. In this case, the tentatively negative relation between UV/optical variability and radio emission in RQs reported in this work may support the scenario that the radio emission in RQs is dominated by weak jet. Future studies of larger RQQ samples may reveal whether the tentatively negative relation is statistically robust, providing new clues to the radio emission origin.

The large-scale radio emission from star formation in the host galaxies may also fit our results (i.e., no statistically significant difference in radio emission between low- and high-variability quasars), as the accretion disk variations caused by random fluctuation may be no relevance with the host properties due to the origin of radio emission at spatial scales different by a factor of several orders. The scenario of star formation origin in RQs is supported by recent low frequency radio observations. With Low Frequency Array (LOFAR; van Haarlem et al. 2013) Two-metre Sky Survey (LoTSS DR1; Shimwell et al. 2017), Gürkan et al. (2019) found that the 144 MHz continuum emission of RQs (quasars with $0.1 < L_{144\text{MHz}}/L_{\text{band}} < 100$) is consistent with being dominated by star formation based on the far-IR to radio correlation measured in local star-forming galaxies (but note the far-

IR to radio correlation may evolves with redshift). However, the weak jet contribution to 144 MHz radio emission in RQs might also be non-negligible. Through modeling the LoTSS radio luminosity distribution of quasars assuming both jet and star formation contribute to radio emission in every quasar, Macfarlane et al. (2021) showed that the radio emission from jets is contributing down at least to the level comparable to the radio emission from star formation.

To summarize, we find more variable RQs (at matched redshift, luminosity and SMBH mass) tend to have tentatively weaker radio emission, disfavoring the corona origin of radio radiation in RQs. If the tentatively negative relation between UV/optical variability and radio emission in RQs could be confirmed in the future, the weak jet origin would be preferred (or at least with significant contribution), as radio emission from star formation is expected to be irrelevant to the short term disc turbulence in quasars.

4.2 Why no directly explore the connection between X-ray and radio emission in RQs?

We have shown that RQs with stronger UV/optical variability, which are known to have relatively stronger X-ray emission, do not show stronger radio emission. This poses clear challenge to the corona origin of the radio emission in RQs. One might ask a simple question: why not directly explore the connection between X-ray and radio emission in RQs?

First of all, the direct correlation between X-ray and radio power in RQs may not yield useful constraints to the radio emission origin. Numerous previous statistical studies have revealed correlations between radio and X-ray emission in RQs and RQ AGN (e.g., Brinkmann et al. 2000; Salvato et al. 2004; Panessa et al. 2007; Laor & Behar 2008; Panessa et al. 2015), seeming to support that their radio emission associates with the central engine of black hole activity instead of the star formation of host galaxies. This however does not necessarily support the corona origin of radio emission in radio-quiet AGN, because if the radio emission comes from jet, it is also expected to correlate with the bolometric power of AGN. Furthermore, studies also revealed correlations between the star formation rate and AGN power in radio-quiet AGN (e.g. Sargent et al. 2010; Thean et al. 2001; Macfarlane et al. 2021), thus the correlation between radio emission and AGN power in radio-quiet sources does not necessarily imply an accretion related origin of the radio emission either.

What if we explore the relation between radio and X-ray emission in RQs after controlling the effect of bolometric luminosity? Intuitively, this could be more straightforward than exploring the relation between UV/optical variability and radio emission. However, as we will show below, this approach is biased thus disfavored compared with the one adopted in this work.

For illustration, we explore the correlation between X-ray and radio emission in RQs (controlling the effect of bolometric luminosity) with an X-ray detected SDSS quasar sample (without requiring variability measurement). We cross-match the fourth XMM-Newton serendipitous source catalogue (4XMM-DR9, Webb et al. 2020) with high SDSS DR7 quasar catalog of Shen et al. (2011) within $5''$, resulting 4252 quasars with X-ray detection(s) where we only retain the one detection with the highest values of maximum-likelihood for those sources that have multiple detections. 4153 out of them fall in the coverage of FIRST survey, and they are further cross-matched with FIRST catalog within $5''$ to exclude potential radio-loud quasars. We find and exclude 485 quasars with FIRST detections, i.e., a fraction of $\sim 11\%$. We perform multiple linear regression to derive the dependence of X-ray (0.2–12 keV) luminosity on z , M_{BH} , and R_{edd} (similar to Equation 2). We then divide the X-ray detected RQs sam-

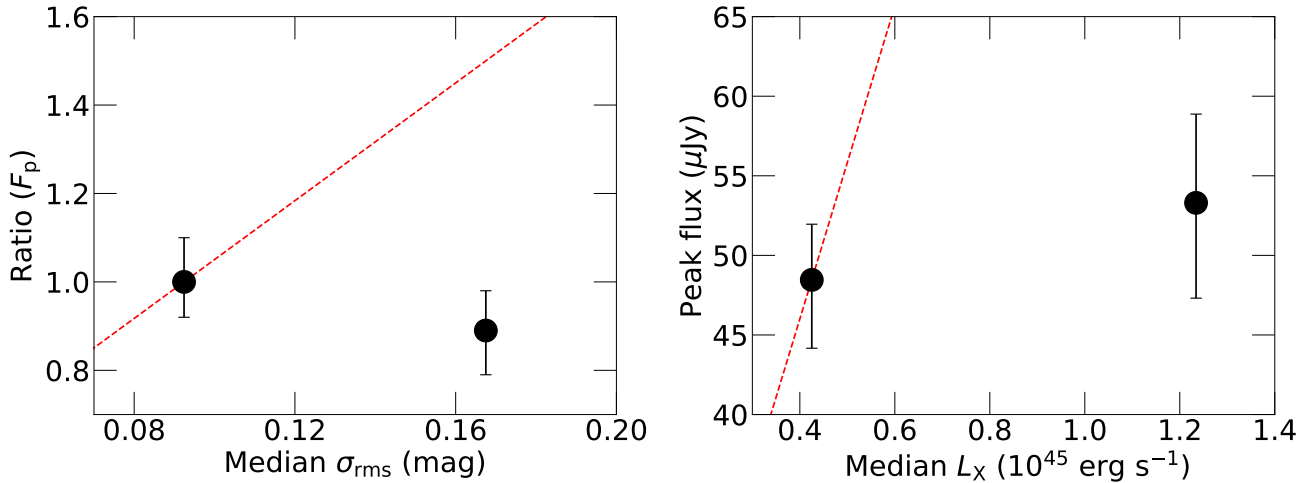


Figure 7. Left: comparison between our results (the median radio flux density ratios, i.e., scaled to LVQ2, versus σ_{rms} of our HVQ2 and LVQ2, black dots), and the prediction relation (red dashed line) based on the measured relation between X-ray loudness and σ_{rms} from Kang et al. (2018) and assuming a linear radio/X-ray relation. Right: the detected median radio flux densities versus median X-ray luminosity of two X-ray detected RQQ samples (black dots); the red dashed line mark the linear radio/X-ray relation.

ple equally into X-ray brighter and X-ray-fainter subsamples, based on their residual X-ray luminosity with respect to the expected values derived from the best-fit regression. The K-S test results demonstrate that these two subsamples already have statistically indistinguishable distributions of z , M_{BH} , L_{bol} and R_{edd} . We find median peak flux densities $53.3^{+5.6}_{-6.0} \mu\text{Jy}$ and $48.5^{+3.5}_{-4.3} \mu\text{Jy}$ in X-ray brighter and X-ray-fainter subsamples⁷, respectively, also contrary to a linear correlation between X-ray and radio emission (see the right panel of Fig. 7).

But note that the X-ray brighter sample here yield slightly higher radio emission compared with the X-ray fainter sample, while our HVQ sample which is X-ray brighter than LVQ sample exhibits slightly lower radio emission than LVQ, although neither the differences is statistically significant. The subtle inconsistency between the two approaches could be due the uncertainties in bolometric luminosity or Eddington ratio. This is because the observed bolometric luminosity of an individual source could significantly deviate from the intrinsic value because of flux variability or inclination effect of the accretion disc emission, and since both radio and X-ray power correlates with the central engine, the uncertainties in bolometric luminosity could lead artificial partial correlations between radio and X-ray emission (e.g. Kang et al. 2018). Though the results from two approaches are generally consistent, as the dependence of variability on bolometric luminosity is much weaker than that of X-ray or radio power (e.g., see Fig. 2 in Kang et al. 2018), the primary approach presented in this work provides less biased results and thus is preferred.

ACKNOWLEDGEMENTS

We thank the anonymous referee for constructive suggestions which is great helpful in improving the manuscript. We thank Richard L. White, Xiaofeng Li, Mladen Novak, Zhengyi Cai, Lu Shen, Zesen Lin for useful discussions. This work was supported by the National

Science Foundation of China (Grants No. 1890693, 12033006 & 12192221), the China Postdoctoral Science Foundation (Grant No. 2021M693089), and the CASFrontier Science Key Research Program (QYZDJ-SSW-SLH006). MHZ is supported by the Science and Technology Project funded by the Education Department of Jiangxi Province in China (Grant No. GJJ211733), and the Doctoral Scientific Research Foundation of Shangrao Normal University (Grant No. K6000449).

DATA AVAILABILITY

This work is based on public images available from the FIRST and Stripe82 VLA archive.

REFERENCES

- Ananna T. T., et al., 2017, *ApJ*, 850, 66
- Baldi R. D., Laor A., Behar E., Horesh A., Panessa F., McHardy I., Kimball A., 2021, arXiv e-prints, p. arXiv:2107.14490
- Becker R. H., White R. L., Helfand D. J., 1995, *ApJ*, 450, 559
- Behar E., Vogel S., Baldi R. D., Smith K. L., Mushotzky R. F., 2018, *MNRAS*, 478, 399
- Blandford R. D., Königl A., 1979, *ApJ*, 232, 34
- Blandford R., Meier D., Readhead A., 2019, *ARA&A*, 57, 467
- Blundell K. M., Beasley A. J., 1998, *MNRAS*, 299, 165
- Blundell K. M., Rawlings S., 2001, *ApJ*, 562, L5
- Blundell K. M., Beasley A. J., Bicknell G. V., 2003, *ApJ*, 591, L103
- Bonzini M., et al., 2015, *MNRAS*, 453, 1079
- Brinkmann W., Laurent-Muehleisen S. A., Voges W., Siebert J., Becker R. H., Brotherton M. S., White R. L., Gregg M. D., 2000, *A&A*, 356, 445
- Cai Z.-Y., Wang J.-X., Gu W.-M., Sun Y.-H., Wu M.-C., Huang X.-X., Chen X.-Y., 2016, *ApJ*, 826, 7
- Cai Z.-Y., Wang J.-X., Zhu F.-F., Sun M.-Y., Gu W.-M., Cao X.-W., Yuan F., 2018, *ApJ*, 855, 117
- Cai Z., Sun Y., Wang J., Zhu F., Gu W., Yuan F., 2019, *Science China Physics, Mechanics, and Astronomy*, 62, 69511
- Falcke H., Biermann P. L., 1995, *A&A*, 293, 665
- Garn T., Alexander P., 2009, *MNRAS*, 394, 105

⁷ Here, the peak flux densities is directly from the median (50th percentile) of the quasars after excluding the $\sim 11\%$ radio detected ones.

Guedel M., Benz A. O., 1993, *ApJ*, 405, L63
 Gürkan G., et al., 2019, *A&A*, 622, A11
 Hardcastle M. J., Croston J. H., 2020, *New Astron. Rev.*, 88, 101539
 Helfand D. J., White R. L., Becker R. H., 2015, *ApJ*, 801, 26
 Hodge J. A., Becker R. H., White R. L., Richards G. T., Zeimann G. R., 2011, *AJ*, 142, 3
 Hwang H.-C., Zakamska N. L., Alexandroff R. M., Hamann F., Greene J. E., Perrotta S., Richards G. T., 2018, *MNRAS*, 477, 830
 Inoue Y., Doi A., 2018, *ApJ*, 869, 114
 Ivezić Ž., et al., 2002, *AJ*, 124, 2364
 Kang W.-y., Wang J.-X., Cai Z.-Y., Guo H.-X., Zhu F.-F., Cao X.-W., Gu W.-M., Yuan F., 2018, *ApJ*, 868, 58
 Kang W.-Y., Wang J.-X., Cai Z.-Y., Ren W.-K., 2021, *ApJ*, 911, 148
 Karim A., et al., 2011, *ApJ*, 730, 61
 Kellermann K. I., Sramek R., Schmidt M., Shaffer D. B., Green R., 1989, *AJ*, 98, 1195
 Kellermann K. I., Sramek R. A., Schmidt M., Green R. F., Shaffer D. B., 1994, *AJ*, 108, 1163
 Kellermann K. I., Condon J. J., Kimball A. E., Perley R. A., Ivezić Ž., 2016, *ApJ*, 831, 168
 Kelly B. C., Bechtold J., Siemiginowska A., 2009, *ApJ*, 698, 895
 Kukula M. J., Dunlop J. S., Hughes D. H., Rawlings S., 1998, *MNRAS*, 297, 366
 Laor A., Behar E., 2008, *MNRAS*, 390, 847
 Leipski C., Falcke H., Bennert N., Hüttemeister S., 2006, *A&A*, 455, 161
 MacLeod C. L., et al., 2012, *ApJ*, 753, 106
 Macfarlane C., et al., 2021, *MNRAS*, 506, 5888
 Miller P., Rawlings S., Saunders R., 1993, *MNRAS*, 263, 425
 Mullaney J. R., Alexander D. M., Fine S., Goulding A. D., Harrison C. M., Hickox R. C., 2013, *MNRAS*, 433, 622
 Neupert W. M., 1968, *ApJ*, 153, L59
 Olsson E., Aalto S., Thomasson M., Beswick R., 2010, *A&A*, 513, A11
 Padovani P., 2016, *A&ARv*, 24, 13
 Padovani P., 2017, *Nature Astronomy*, 1, 0194
 Padovani P., et al., 2017, *A&ARv*, 25, 2
 Panessa F., Giroletti M., 2013, *MNRAS*, 432, 1138
 Panessa F., Barcons X., Bassani L., Cappi M., Carrera F. J., Ho L. C., Pellegrini S., 2007, *A&A*, 467, 519
 Panessa F., et al., 2015, *MNRAS*, 447, 1289
 Panessa F., Baldi R. D., Laor A., Padovani P., Behar E., McHardy I., 2019, *Nature Astronomy*, 3, 387
 Radcliffe J. F., Barthel P. D., Garrett M. A., Beswick R. J., Thomson A. P., Muxlow T. W. B., 2021, *A&A*, 649, L9
 Raginski I., Laor A., 2016, *MNRAS*, 459, 2082
 Salvato M., Greiner J., Kuhlbrodt B., 2004, *ApJ*, 600, L31
 Sargent M. T., et al., 2010, *ApJS*, 186, 341
 Sesar B., et al., 2007, *AJ*, 134, 2236
 Shen Y., et al., 2011, *ApJS*, 194, 45
 Shimwell T. W., et al., 2017, *A&A*, 598, A104
 Smith K. L., et al., 2020, *MNRAS*, 492, 4216
 Thean A., Pedlar A., Kukula M. J., Baum S. A., O’Dea C. P., 2001, *MNRAS*, 325, 737
 Thompson A. R., Moran J. M., Swenson George W. J., 2017, *Interferometry and Synthesis in Radio Astronomy*, 3rd Edition
 Ulvestad J. S., Antonucci R. R. J., Barvainis R., 2005, *ApJ*, 621, 123
 Wang A., An T., Jaiswal S., Mohan P., Wang Y., Baan W. A., Zhang Y., Yang X., 2021, *MNRAS*, 504, 3823
 Webb N. A., et al., 2020, *A&A*, 641, A136
 White R. L., Helfand D. J., Becker R. H., Glikman E., de Vries W., 2007, *ApJ*, 654, 99
 White S. V., Jarvis M. J., Kalfountzou E., Hardcastle M. J., Verma A., Cao Orjales J. M., Stevens J., 2017, *MNRAS*, 468, 217
 Zakamska N. L., Greene J. E., 2014, *MNRAS*, 442, 784
 Zakamska N. L., et al., 2016, *MNRAS*, 455, 4191
 Zhou M.-H., Gu M.-F., 2021, *Research in Astronomy and Astrophysics*, 21, 004
 Zuo W., Wu X.-B., Liu Y.-Q., Jiao C.-L., 2012, *ApJ*, 758, 104
 van Haarlem M. P., et al., 2013, *A&A*, 556, A2

van der Walt S., Colbert S. C., Varoquaux G., 2011, *Computing in Science and Engineering*, 13, 22

This paper has been typeset from a \LaTeX file prepared by the author.